34th Fluid Dynamics Conference and Exhibit
28 June-1 July, 2004/ Portland, OR.

AIAA-2004-2432

Large-Eddy Simulation of the Tip Flow of a Rotor in Hover

Reza Ghias*, Rajat Mittal† , Haibo Dong‡
Department of Mechanical and Aerospace Engineering
The George Washington University, Washington, DC 20052,

and

Thomas S. Lund§
Department of Aerospace Engineering Sciences
The University of Colorado at Boulder, Boulder, CO 80309-0429

An efficient and flexible parallel version of a Large-Eddy Simulation (LES) solver has been developed to simulate the compressible tip-flow of a rotor in hover. The solver employs an immersed-boundary technique in conjunction with a curvilinear structured grid and the dynamic model is used to model the subgrid scale (SGS) stress terms. The solver also employs a hybrid implicit-explicit time-discretization scheme wherein the diagonal viscous terms are treated implicitly and all other terms including the convective terms and cross-terms are treated explicitly using a low-storage 3rd-order Runge-Kutta scheme. A mixed second-order central-difference-QUICK scheme has been used which allows us to precisely control the numerical damping. Preliminary results from non-rotating tip-flow are presented.

I. Introduction

The blade-tip vortex is one of the most important aerodynamic features of a helicopter rotor wake. The strength, size, location and orientation of the tip vortices have a direct impact on rotor performance and blade loading. In addition, in some flight configurations, blade-vortex interaction (BVI) can result in rotor noise and vibration. The tip-vortices can also interact with the airframe and cause undesirable vibration, noise and degradation in the handling qualities of the helicopter. An understanding of tip-vortex formation and evolution is a necessary precursor to developing blade-tip designs that can diminish these undesirable characteristics of the tip vortex. Experimental investigation of the tip-vortex is however difficult because of the need to operate in the vicinity of a high speed rotating rotor, the problem of setting up the correct far field conditions, and adequately seeding the vortex core for flow visualization. Despite this, a few detailed experimental investigations of the rotor tip vortex have been undertaken by Leishman and Bagai[1], Bhagwat and Leishman[2], McAlister et al.[3], and Thomson et al.[4]among others.

Accurate numerical simulation of tip-flow is also a difficult proposition. Turbulent diffusion and dissipation have a significant effect on the size and intensity of the tip-vortex and have to be modeled with reasonable accuracy.[5] Most of the numerical simulations in the past have employed dissipative schemes in conjunction with relatively coarse meshes, which cause inaccurate prediction of the size, location and strength of the tip-vortex. Furthermore, the flow in the tip vortex is highly unsteady, three-dimensional and non-homogeneous and contains a wide range of spatial and temporal scales. Thus, simple Reynolds Averaged-Navier-Stokes (RANS) approaches which are designed to solve for the steady state, time-averaged velocity and pressure field[6,7], are not expected to perform well in predicting this flow.

Large-eddy simulation, with the dynamic subgrid-scale model[8,9] is an approach which is well suited for this type of flow problem. The LES methodology falls somewhere between the Direct Numerical Simulation (DNS) and RANS[10] approaches. In LES the large energy-containing scales are resolved and only outcome of the small, unresolved (subgrid) scales is modeled. Dynamic SGS modeling is an approach in which a procedure for

* Graduate Research Assistant, Student Member AIAA
† Associate Professor, Senior Member AIAA.
‡ Research Scientist, Member AIAA.
§ Visiting Professor, Member AIAA.

dynamically calculating the model constant is added on to the SGS model.[8,9] As the calculation proceeds, the dynamic procedure utilizes information from the smallest resolved scales to predict the energy transfer to subgrid scales. The model constant is then computed from the estimated rate of energy transfer. The dynamic model is ideally suited for complex flows, since it automatically detects laminar regions and turns itself off. This modeling technique has been used successfully to simulate a variety of flows.[9,11-14] Moreover, LES provides detailed time-dependent information about the important large scale features of the flow field without the immense cost of a DNS which would resolve all the scales down to dissipation range.

In addition to providing time-dependent information for a wide range of scales in the flow, the LES approach also offers other advantages for calculation of rotor flow fields. As mentioned earlier, in most current approaches, the vortex core is smeared out due to the coarseness of the mesh and presence of the numerical diffusion. On the other hand, well designed LES calculations are usually carried out with non- (or minimally) dissipative schemes[14] and higher resolution is provided in the wake region to the vortex sheet and tip vortex which reduces truncation error effects. However, the high Reynolds number (10^5-10^6) of this flow constrains such simulations to a limited region that surrounds the blade-tip and the tip-vortex. At the outset, it was estimated that even for this limited region a grid with O(10^7) points would be required and the simulations would have to be run for O(10^5) time steps in order to gather reliable statistics. The CPU requirements for these simulations are therefore enormous making them feasible only on parallel computers. In the current effort, we have developed a parallel LES solver to simulate the compressible tip-flow. The simulations are designed to match the experiments of Martin[15] and Martin *et al.*[16], where a rectangular one-blade rotor with a NACA 2415 section was employed. The blade had a tip radius of 406 mm and a 44.5 mm chord, and was balanced by a counterweight. The rotational frequency was set to 35.0 Hz ($\Omega = 70\pi$ rad/sec). This led to a rotor-tip speed of 89.28 m/s which corresponds to a tip Mach number and chord Reynolds number of 0.26 and 272,000 respectively. All the tests were conducted for an effective blade loading of $C_T/\sigma = 0.064$ using a collective pitch of 4.5° where C_T and σ are rotor thrust coefficient and rotor solidity respectively. High resolution three-dimensional velocity field measurement and flow visualization in the rotor-tip vortex were obtained using Laser Doppler Velocimetry (LDV).

The experimental data allow us to validate our solver. Once validated the LES data can be employed to gain a better understanding of the tip flow. In the current paper we will provide a detailed description of the numerical method and preliminary results from non-rotating tip-flow simulations.

II. Numerical Methodology

A. Governing Equations

The governing equations are unsteady, viscous, compressible Navier-Stokes equations written in terms of conservative variables. The continuity, momentum and energy equations are:

$$\frac{\partial}{\partial t}\overline{\rho} + \frac{\partial}{\partial x_k}\left(\overline{\rho u_k}\right) = 0$$

$$\frac{\partial}{\partial t}\left(\overline{\rho u_i}\right) + \frac{\partial}{\partial x_k}\left(\overline{\rho u_k}\,\overline{u}_k + \overline{p}\,\delta_{ik} - \overline{\sigma}_{ik} + \tau_{ik}\right) = F_i^{\Omega}$$

$$\frac{\partial}{\partial t}\overline{e} + \frac{\partial}{\partial x_k}\left[\overline{u}_k\left(\overline{e} + \overline{p}\right) - \overline{\sigma}_{ik}\,\overline{u}_i + \overline{Q}_k + \overline{q}_k\right] = 0$$

where, the molecular heat flux and stress tensors are given by

$$Q_k = -\frac{\gamma}{(\gamma - 1)\mathrm{Re}\,\mathrm{Pr}}\frac{\partial T}{\partial x_k} \quad \text{and}$$

$$\sigma_{ik} = \frac{1}{\mathrm{Re}}\left(\frac{\partial u_i}{\partial x_k} + \frac{\partial u_k}{\partial x_i}\right) - \frac{2}{3}\frac{1}{\mathrm{Re}}\delta_{ik}\frac{\partial u_j}{\partial x_j}$$

respectively and F_i^{Ω} is the force associated with rotation. In the above equations, Pr is the Prandtl number and Re is the Reynolds number. The velocity components and the pressure are related to the total energy per unit volume through the equation of state for a perfect gas by

$$e=\frac{p}{(\gamma-1)}+\frac{1}{2}\rho u_k u_k$$

The bar in the above equations indicates the resolved quantities, i.e. those scales that are represented on the given mesh. Furthermore, in the above equations, τ and q are the subgrid-scale stress and heat flux respectively which are defined as:

$$\tau_{ij}=\overline{\rho u_k u_i}-\frac{\overline{\rho u_i}}{\overline{\rho}}\overline{\rho u_k}$$

$$q_{ij}=\overline{p u_k}-\frac{\overline{\rho u_k}}{\overline{\rho}}\overline{p}$$

B. Subgrid-Scale Model

Closure in the above equations is provided by modeling the SGS stress and heat flux terms. A trace-free Smagorinsky model[17] is used for modeling the SGS stress and Yoshizawa's[18] model is used for parameterization of SGS energy (τ_{kk}) wherein

$$\tau_{ij}-\frac{\delta_{ij}}{3}\tau_{kk}=-2C\overline{\rho}\Delta^2\left|\overline{S}\right|\left(\overline{S_{ij}}-\frac{\delta_{ij}}{3}\overline{S_{kk}}\right)$$

$$\tau_{kk}=2C_I\overline{\rho}\Delta^2\left|\overline{S}\right|$$

In the above equations, $\boldsymbol{S}$ is the strain rate tensor, Δ is the grid spacing, C is the Smagorinsky's constant, and C_I is the SGS energy coefficient. The SGS heat flux is modeled as

$$q_k=-\overline{\rho}\frac{C\overline{\rho}\Delta^2\left|\overline{S}\right|}{\mathrm{Pr}_t}\frac{\partial\overline{T}}{\partial x_k}$$

where Pr_t is the turbulent Prandtl number. The key feature of the dynamic model is that it provides a formula for calculating C, C_I and Pr_t directly from the resolved flow quantities. This procedure is explained by Moin et al. [9] and El-Hady et al.[13]for compressible flows.

Since the tip-flow is completely inhomogeneous, the conventional dynamic model which relies on the presence of a homogeneous direction, cannot be employed. There are two other implementations of the dynamic model which are suitable for fully inhomogeneous flow; the dynamic localization model of Ghosal *et al.*[19] and the Lagrangian dynamic model (LDM) of Meneveau *et al.*[20] The latter, which is computationally less expensive is used in our simulation. In this model, the Smagorinsky's coefficient is obtained by averaging along particle trajectories and therefore the implementation does not require the presence of a homogenous averaging direction.

C. Discretization of the Governing Equations

The equations are transformed to a generalized curvilinear coordinate system, (ξ,η,ζ) while maintaining the strong conservation form of the equations[21]. The equations are discretized in this computational domain with a cell-centered arrangement using a hybrid second-order central-difference-QUICK scheme[22] which is introduced in the split fluxes[23]. The weight factor for each scheme can be adjusted and allows us to precisely control the numerical dissipation. The diagonal viscous terms are treated implicitly using a Crank-Nicolson scheme wherein all the other terms including the convective terms and cross-terms are treated explicitly using a low-storage, 3rd –order Runge-Kutta scheme.[24] Use of this mixed implicit-explicit scheme virtually eliminates the viscous stability constraint which can be quite severe in simulation of viscous flows. The resulting equations are solved by a LSOR iterative method.[21]

D. Mesh Topology and Immersed Boundary Method.

As shown by Mittal *et al.*[14], it is crucial that LES be coupled with non-dissipative numerical schemes such as the second-order central difference used in the current effort. A consequence of using non-dissipative schemes is that simulations become very sensitive to the quality of the mesh as aptly demonstrated.[25] Tip-flow simulations are usually carried out with a C-H type mesh[26] but this type of mesh has a four branch cuts where grid quality is usually

quite poor. We have circumvented this issue by using the so-called "Immersed Boundary Method (IBM)". The key feature of this method is that flow past immersed boundaries can be simulated on structured curvilinear grids that do not conform to the shape of the boundaries and this allows us to simulate this flow on a single-block mesh with no branch cuts. The use of this topologically simple grid allows us to maintain relatively better grid quality in the entire domain. In the current method, the geometry of immersed boundary is defined by a set of marker points. Cells whose centers lie inside the immersed body and have at least one neighboring cell whose cell-center lies outside the body, are marked as "ghost-cells". The rest of the cells with centers inside the body, which are not adjacent to immersed boundary, are marked as "solid" cells. Fig.1 shows the marker points, fluid cells, ghost cells and solid cells for an immersed boundary on a Cartesian grid. The basic idea in this method is to compute the flow variables for the ghost cells such that boundary conditions on the immersed boundary in the vicinity of the ghost cell are satisfied.

The advantage of this approach for the current tip flow is that since the blade does not vary in shape across the span, we can simply use a planar mesh in the spanwise direction (Fig.2). This greatly simplifies the mesh topology and discretization and gives us much more precise control over the grid quality. The use of a curvilinear mesh still allows us control over the grid resolution in localized regions such as boundary layers. Fig. 3 shows the grid of 460 x179 in *x-y* plane which is used for simulation of tip flow around a NACA 2415 airfoil. Since the surface of the airfoil is mostly represented by the longitudinal grid lines, this allows us to provide a higher resolution selectively in the boundary layer region. A similar approach has been used for incompressible tip-clearance flow simulations.[27] Accuracy tests and validation of this solver against established experiments and simulations has been described in detail in previous paper. [28]

E. Parallelization of the solver

An efficient and flexible Message-Passing Interface (MPI) based parallel version of the solver has been developed for the tip-flow simulations. In the algorithm adopted, the computational domain is decomposed into several sub-domains in the stream wise direction. Each sub-domain is enclosed with a layer of overlapping points. These overlapping points store flow variables transferred from the neighboring sub-domain for the solution of variables within the sub-domain. The key feature of the domain decomposition is the implementation of the LSOR iterative method that is used to solver the transport equations. The method currently adopted employs a Jacobi iteration at the domain interfaces but retains a Gauss-Siedel approach for all the nodes inside a given domain. Tests indicate that the convergence properties of the iterative method do not deteriorate due to this procedure. Figure 4 shows streamwise velocity contours around airfoil NACA2415. Our parallel code has been successfully tested on a 16-CPU in-house Beowulf cluster which is based on a 2.8 GHz Pentium-4 processor and employs a gigabit interconnect between the nodes. Extensive tests show that the parallel code achieves reasonably good parallel efficiency (see Figure 5) for grid sizes that are relevant for the tip-flow simulations.

F. Tip-Flow Configuration

The flow configuration is schematically shown in Fig. 6. As mentioned before, the experimental configuration that we have chosen is the one that was the subject of the detailed study by Martin.[15] .The computational domain is of size L_x x L_y x L_z = 3.5C x 4.0C x 3.0C, where C is the chord length. Due to the high Reynolds number and the need to resolve the wake and tip-vortex, we extended the domain size 1.0C upstream of the leading edge and 1.0C downstream of the trailing edge. Thus in this simulation we should be able to capture the wake with age up to 5 degrees with enough resolution in the streamwise (*x*) direction. The vertical (*y*) extent of the domain is such that the boundary layer grows naturally with minimum effect from the vertical boundary. The choice of the spanwise domain size is driven by the size of the tip-vortex and the fact that far enough from the tip of the airfoil there is not much variation in the spanwise *(z*) direction. Thus the spanwise domain size is extended 1.0*C* and 2.0*C* on the inward and outward of the blade tip respectively. The simulation is performed in a reference-frame attached to the rotor which eliminates the need to incorporate a moving boundary in computation.

The flow is assumed to be compressible with constant specific heat ratio. At the inflow, all velocity components as well as the temperature are imposed, while the density is extrapolated from the domain and pressure is calculated by using the equation of state. At the outflow, a non-reflecting Navier-Stokes characteristic boundary condition[29] is used which allows vortex structures to exit the computational domain with minimal spurious reflections. The lateral boundaries are treated as moving walls, and density and temperature are determined by assuming adiabatic wall condition. The no-slip boundary condition is imposed at the surface of circular cylinder. Zero-stress boundary conditions at the inner spanwise boundary and free stream conditions are imposed at the outer spanwise boundary.

III. Numerical Results and Discussion

G. 2D NACA 2415 Flow Simulations

The objective of these simulations was to explore the grid requirements and solver performance of the flow at high Reynolds numbers over the blade mid-span where the flow is expected to be nominally two-dimensional. Furthermore, these simulations also allow us to gauge the feasibility of the immersed boundary approach for this flow. Simulations have been carried out at a chord-based Reynolds number of 272,000 and Mach number 0.26 which matches with the experiment described earlier. For this simulation, a 532×379 curvilinear grid is used with a QUICK weight factor of 0.5. Figures 7-10 show visualizations of spanwise vorticity, pressure, temperature and Mach number contours for this flow respectively. The key observation here is that the wake vortices seem to convect for over a chord length into the wake without excessive dissipation. This provides some confirmation of the favorable numerical dissipation characteristics of the numerical scheme employed. It should be pointed out that these simulations were run on seven processors of a 2.8 GHz Pentium Linux Beowulf cluster.

H. Rotor Tip-Flow Simulations

The 2D simulations allow us to design a mesh for the tip-flow simulations. Two different meshes with $460 \times 179 \times 61$ and $460 \times 179 \times 149$ grid points have been employed. The coarser grid simulation was carried out first and the results of this simulation indicated that the spanwise structure of the tip-vortex was inadequately resolved. This led to the second mesh, which has a much higher resolution in this direction. It should be noted that this finer mesh has over twelve million mesh points and requires almost 20,000 single-node CPU hours on a 2.8 GHz Pentium-4 per chord-flow time. This first set of simulations has been carried out at a lower Reynolds number of 100,000. The Mach number is however 0.26 which matches the experiment.

Figures 11 (a,b) show isosurface of streamwise vortices and enstrophy contours in different planes in the wake of the NACA 2415 respectively at a relatively early stage in the simulations where $tU_\infty / C = 0.01$ The plots clearly show the initial stage in the formation of the tip vortex. Figure12 shows the spanwise vortex contours in different planes in spanwise direction. Convection of the vortices in the wake without excessive numerical dissipation can be observed. Furthermore, the flow visualizations shows that downstream of the trailing edge, the tip vortex and blade wake transitions to a complex three-dimensional flow which is the first stage in the transition to turbulence. Plot of eddy viscosity in different planes along the spanwise direction in Fig. 13 clearly shows that eddy viscosity is correctly produced only in regions where the flow is turbulent. Within this region, peak eddy viscosity ranges up to about five times the molecular viscosity.

IV. SUMMARY

In this paper, we have describes an efficient and flexible parallel version of a large-eddy simulation (LES) solver for simulating the compressible tip-flow of a rotor in hover. Preliminary results from an airfoil tip-flow simulation at Re = 100000 have been presented. These simulations are currently proceeding and comprehensive validation against the experiment will be presented in the future.

Acknowledgement

This research is supported by the U.S. Army Research Office Grant No. DAAD 19-01-1-0704 monitored by Dr. T. Doligalski.

References

[1]Lishman, J.G. and Bagai, A., Challenges in Understanding the Vortex Dynamics of Helicopter Rotor Wakes. *AIAA J*. 36, No. 7 (1998) 1130-1140.

[2]Bhagwat, MJ, and Leishman, J.G., Correlation of Helicopter Rotor Tip Vortex Measurements., *AIAA J*., Vol. 38, No. 2(2000) 301-308

[3]McAlister, KW, Schuler, CA, Brannum, L., and Wu, Jc. 3-D wake Measurements Near a Hovering Rotor for Determining Profile and Induced Drag. NASATP 3577(1995).

[4]Thompson, Tl, Komerath, NM and Gray, RB, Visualization and Measurement of the Tip Vortex Core of Rotor Blade in Hover, J. Aircraft, Vol. 25, No.12(1988) 1113-1121.

[5]Srinivasan, G.R. and McCroskey, W.J., " Navier-Stokes Calculations of Hovering Rotor Flow Fields," *J. Aircraft*, Vol. 25, No. 10, (1988), pp. 865-874.

[6]Wake, B.E. and Sankar, L.N., "Solutions of the Navier-Stokes Equations for Flow About a Rotor Blade," *J. Am. Hel. Soc*., 34(2), (1989), pp. 13-23.

[7]Srinivasan, G.R., Baeder, J.D., Obayashi, S, and McCroskey, W.J., "Flow field of a Lifting Rotor in Hover: A Navier-Stokes Simulation*," AIAA J*., Vol. 30, No. 10, (1992), pp 2371-78.

[8]Germano, M., Piomelli, U., Moin, P., and Cabot, W., " A Dynamic Subgrid-Scale Eddy-Viscosity Model," Phys. of Fluids, A3, (1991), pp. 1760-65.

[9]Moin, P., Squires, K., Cabot, W., and Lee, S., " A Dynamic Subgrid-Scale Model for Compressible Turbulence and Scalar Transport," Phys. of Fluids, A3 (11), (1991), pp. 2746-57.

[10]Rogallo, R.S. and Moin, P., "Numerical Simulations of Turbulent Flows," Annu. Rev. Fluid Mech., 16, (1984), pp.99-137.

[11]Beaudan, P., and Moin, P., Numerical experiments on the flow past a circular cylinder at sub-critical Reynolds number., report No. TF-62, Thermo-sciences Division, Department of Mechanical Engineering, Stanford University, (1994).

[12]Kaltenbach, H.J., Fatica, M., Mittal, R., Lund, T.S., and Moin., P., " Study of Flow in an Asymmetric Planar Diffuser Using Large-Eddy Simulation," J. Fluid Mech., 390, (1999), pp. 151-185.

[13]El-Hady, N.M., " Large-Eddy Simulation of Laminar-Turbulent Breakdown at High Speed with Dynamic Subgrid-Scale Modeling," NASA CR 4533., (1993).

[14]Mittal, R., Moin, P., " Suitability of Upwind-Biased Schemes for Large-Eddy Simulation of Turbulent Flows," *AIAA J.,* Vol. 36, No. 8, (1997), pp. 1415-17.

[15]Martin, B. P., " Measurements of The Trailing Vortex Formation, Structure, and Evolutionin The Wake of Hovering Rotor", Doctoral Dissertation, University of Maryland.(2001)

[16]Martin, BP, Pugliese, GJ, and Lieshman , GJ, High Resolution Trailing Vortex Measuremnets in The Wake of a Hovering Rotor., American Helicopter Society, 57th Annual Forum, Washington, DC, May 9-11(2001).

[17]Eelebacher, G., Hussaini, M.Y., Speziale, C.G., and Zang, T.A., "Towards Large-Eddy Simulations of Compressible Turbulent Flows," J. Fluid Mech., 238, (1992), pp. 155-185.

[18]Yoshizawa, A., "Statistical Theory for Compressible Turbulent Shear Flows with the Application to Subgrid Modeling," Phys. Fluids, 29, (1986), pp. 2152.

[19]Ghosal, S., Lund, T.S., Akselvoll, K., and Moin, P.,"A Dynamic Localization Model for Large-Eddy Simulation of Turbulent Flows," J. Fluid Mech., Vol. 286, (1995), pp. 229-255.

[20]Meneveau, C., Lund, T.S., and Cabot, W. H., "A Lagrangian Dynamic subgrid-Scale Model of Turbulence," J. Fluid Mech., 319, (1996), pp. 353-385.

[21]Anderson, A.D., Tannehill, C.J., and Pletcher, R.H., Computational Fluid Mechanics and Heat Transfer, Hemispher Publishing Corporation, New York, 1984, pp. 479-482.

[22]Leonard, B. P., "A stable and accurate on convection modeling procedure based on quadratic upstream interpolation," Computer Methods in Applied Mechanics and Engineering, 19, (1979), pp. 59-98.

[23]Steger, JL, and Warming, RF, "Flux Vector Splitting of Inviscid Gasdynamic Equations with Application to Finite-Difference Methods,"J. of Compu. Phys. No. 40, (1981), pp. 263-293.

[24]Kennedy, C. A., Carpenter, M. A., and Lewis, R. M., "Low-storage, explicit Runge-Kutta scheme for the compressible Navier-Stokes equations," ICASE Report No. 99-22,(1999).

[25]You, D., Wang, M., Mittal, R., Moin, P., **"**Study of rotor tip-clearance flow using large eddy simulation," *AIAA* (2003)-838

[26]Kunz, R. F., Lankshminarayana, B., and Basson, A. H., "Investigation of Tip Clearance Phenomena in an axial Compressor Cascade Using Euler and Navier-Stockes Procedures," ASME J. Turbomach., 115, (1993), pp. 453-467.

[27] You, D., Mittal. R., Wang, M., and Moin, P., "Computational Methodology For Large_Eddy Simulation of Tip-Clearance Flows," AIAA J., Vol. 42, No. 2, (2004), pp. 271-279.

[28]Ghias, R, Mittal, R, and Lund TS, "A Non-Body Conformal Grid Method for Simulation of Compressible Flow with Complex Immersed Boundaries," AIAA2004-0080, Jan. 2004, Reno, NV.

[29]Poinsot, T. J., and Lele, S. K.," Boundary conditions for direct simulations of compressible viscous flows," *J. Comput. Phys.*, 101, (1992), pp. 104-129.

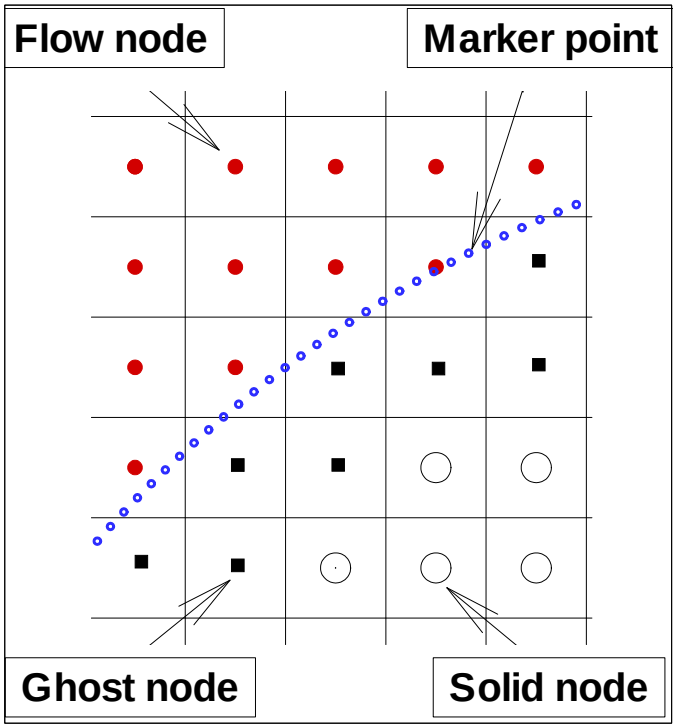

Figure 1: Marker points, flow nodes, ghost nodes and solid nodes in a Cartesian grid.

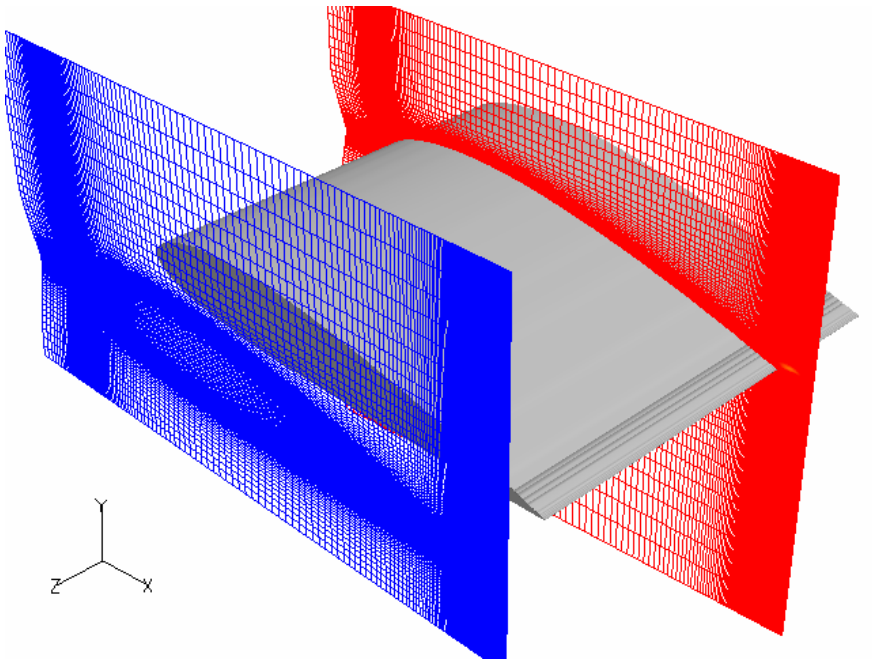

Figure 2: The curvilinear grid which has been repeated in spanwise direction for simulation of the tip flow around NACA 2415 airfoil.

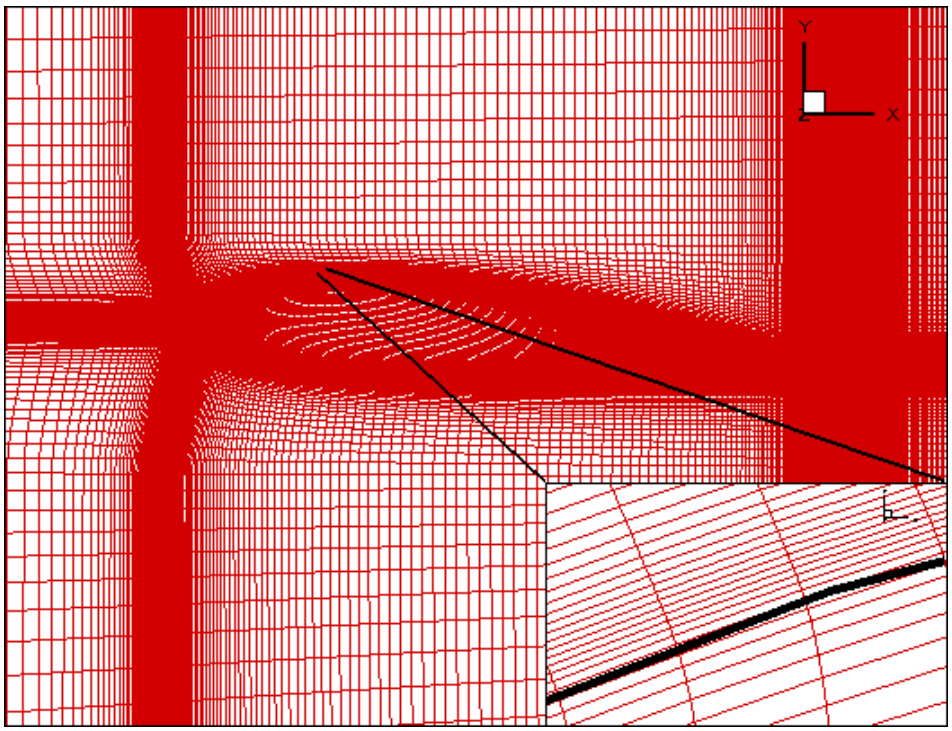

Figure 3: The Rectangular curvilinear domain in *x-y* plane. Grid size is 460 × 197. The black line provides a rough indication of the location of the airfoil surface.

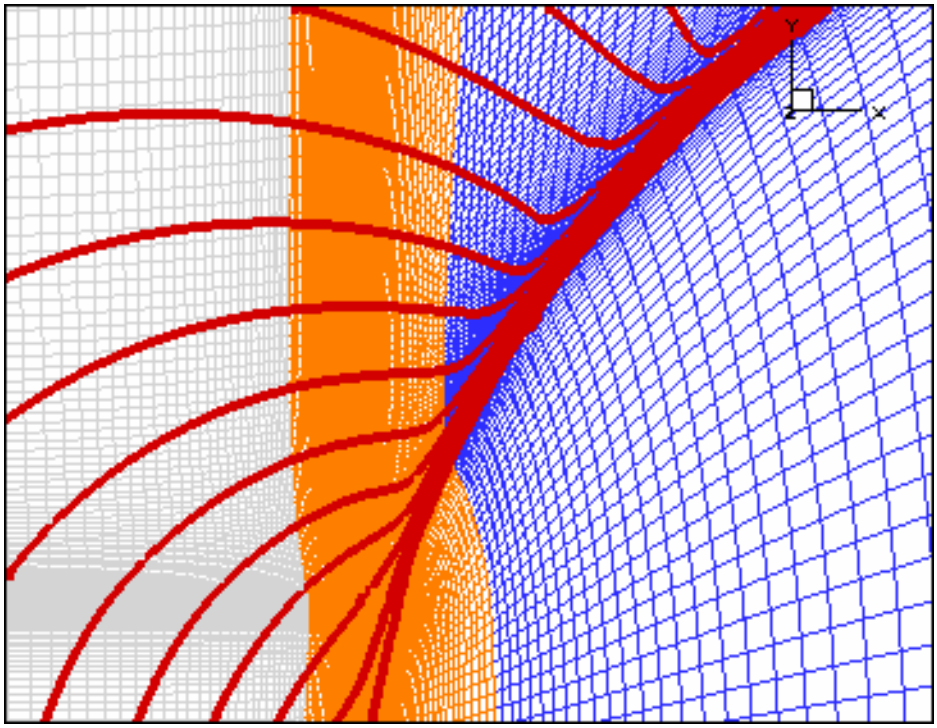

Figure 4: Streamwise velocity contours around airfoil NACA 2415. Three different sub-domains in the grid are visible.

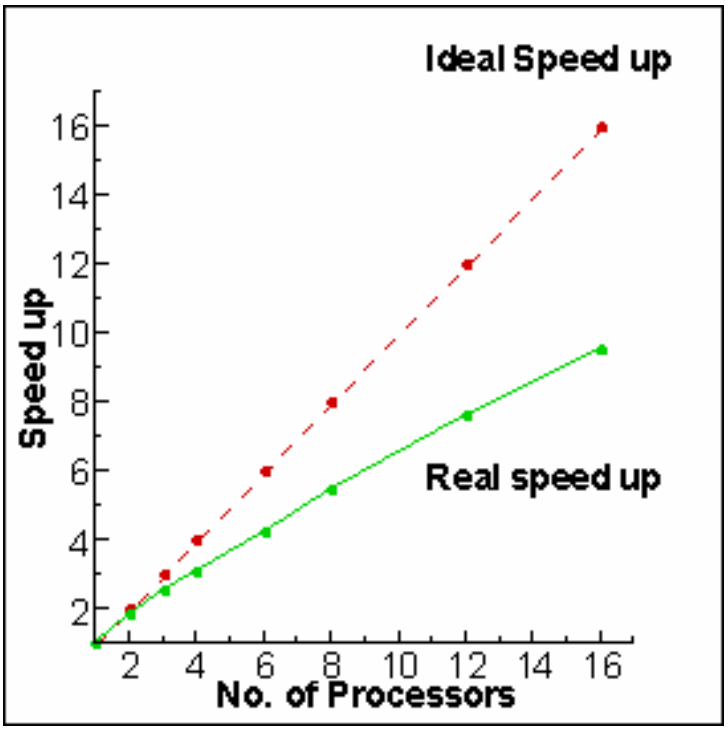

Figure 5: Speed up versus number of the processors.

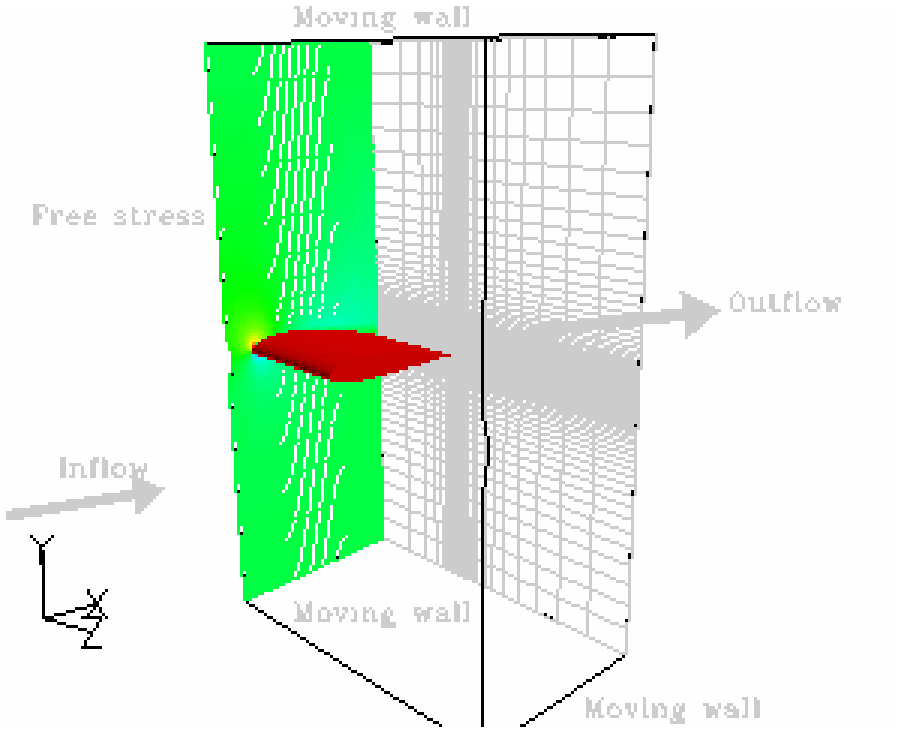

Figure 6: Flow configuration for simulation of tip-flow. The computational domain is L_x x L_y x L_z = 3.5C x 4.0C x 3.0C

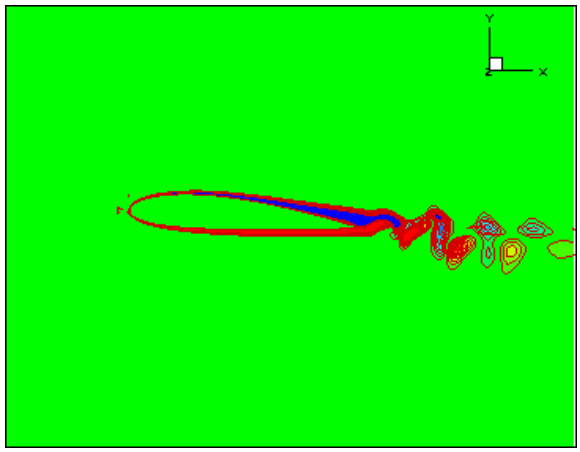

Figure7: Computed spanwise vorticity contours past a NACA 2415 airfoil at AOA = 4.5 ° $\mathrm{Re}_c = 272{,}000$ and $M_\infty = 0.26$

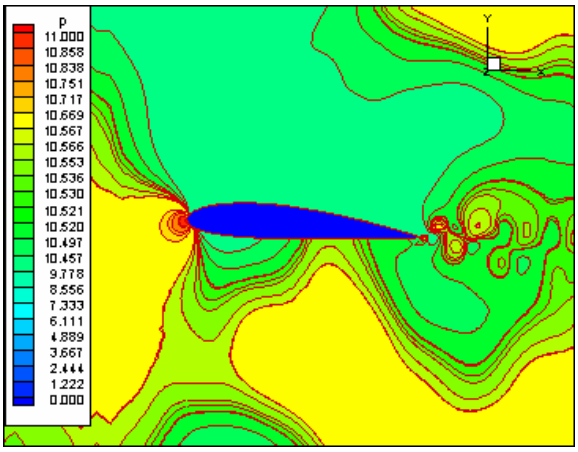

Figure 8: Computed pressure contours, past a NACA 2415 airfoil at AOA = 4.5 °, $\mathrm{Re}_c = 272{,}000$ and $M_\infty = 0.26$

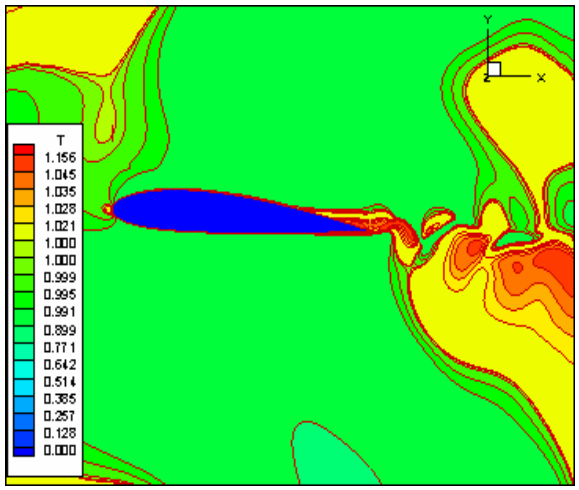

Figure9: Computed temperature contours past a NACA 2415 airfoil at AOA = 4.5 ° $\mathrm{Re}_c = 272{,}000$ and $M_\infty = 0.26$

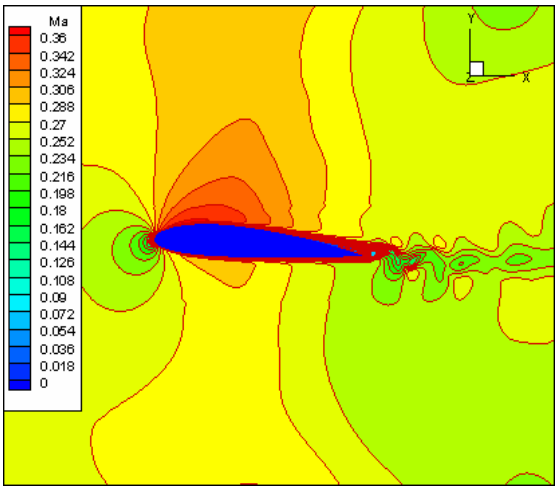

Figure 10: Computed Mach number, past a NACA 2415 airfoil at AOA = 4.5 °, $\mathrm{Re}_c = 272{,}000$ and $M_\infty = 0.26$

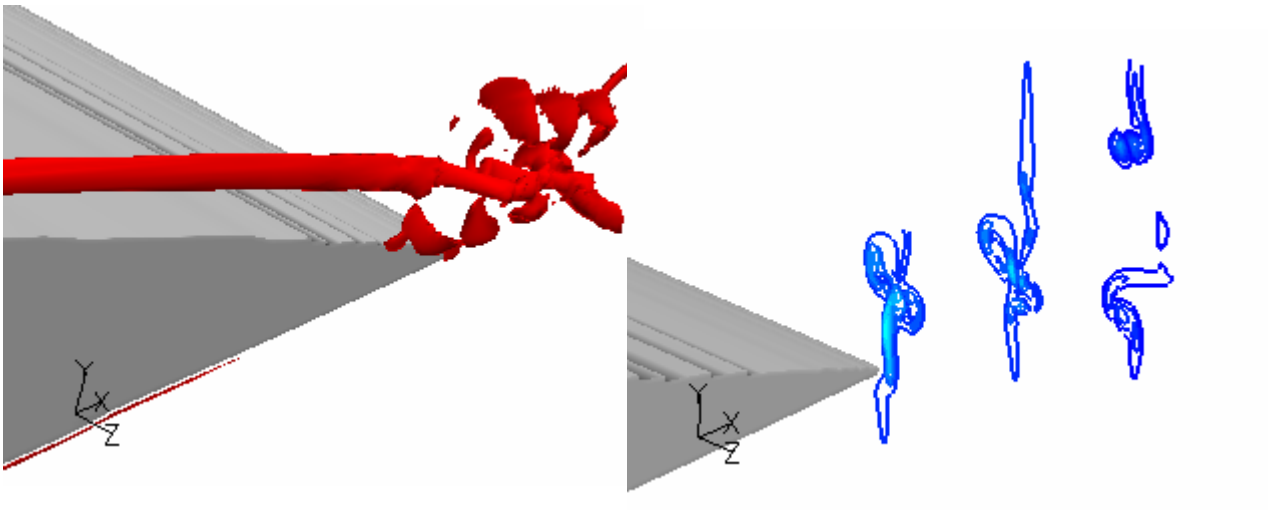

(a) (b)

Figure 11: (a) Iso-surface of streamwise vortices, and (b) enstrophy contours in different planes in the wake of the NACA 2415 respectively for Re = 100,000 and M = 0.26.

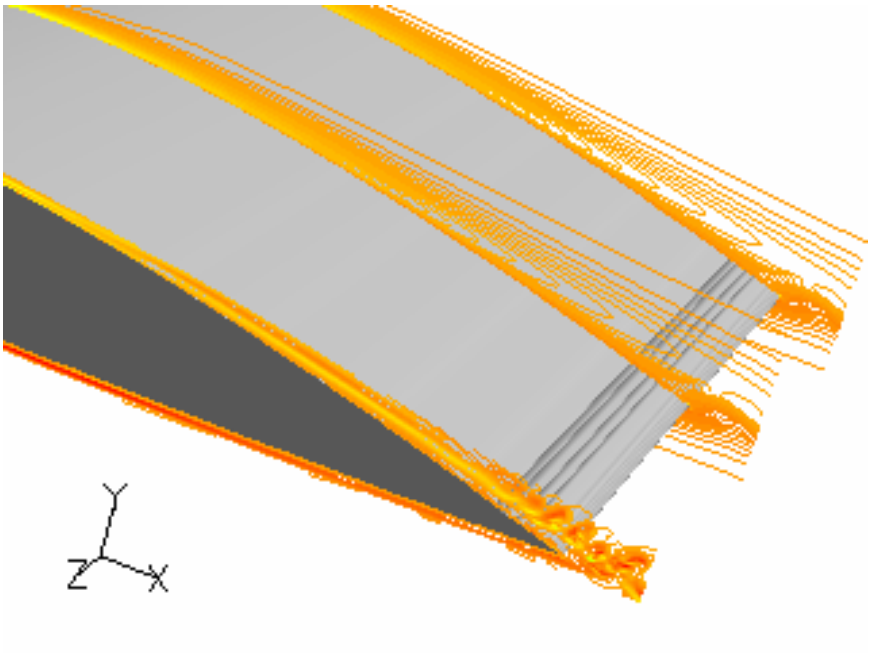

Figure 12: Spanwise vortices contours in different planes in spanwise direction at Re = 100,000

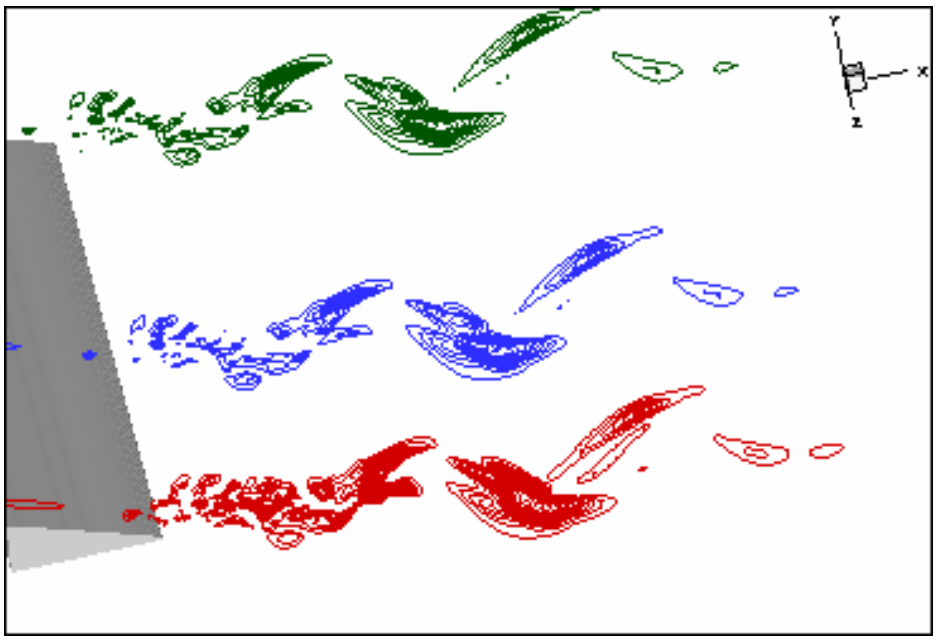

Figure 13: Eddy viscosity contours in the wake near the tail of the airfoil for Re = 100,000 and M = 0.26.